Isolation of Myocardial L-Type Calcium Channel Gating Currents with the Spider Toxin ω-Aga-IIIA

ERIC A. ERTEL, MCHARDY M. SMITH, MARK D. LEIBOWITZ, and CHARLES J. COHEN

From the Department of Membrane Biochemistry and Biophysics, Merck Research Laboratories, Rahway, New Jersey 07065

ABSTRACT The peptide ω-agatoxin-IIIA (ω-Aga-IIIA) blocks ionic current through L-type Ca channels in guinea pig atrial cells without affecting the associated gating currents. ω-Aga-IIIA permits the study of L-type Ca channel ionic and gating currents under nearly identical ionic conditions. Under conditions that isolate L-type Ca channel currents, ω-Aga-IIIA blocks all ionic current during a test pulse and after repolarization. This block reveals intramembrane charge movements of equal magnitude and opposite sign at the beginning of the pulse (Q_{on}) and after repolarization (Q_{off}). Q_{on} and Q_{off} are suppressed by 1 μM felodipine, saturate with increasing test potential, and are insensitive to Cd. The decay of the transient current associated with Q_{on} is composed of fast and slow exponential components. The slow component has a time constant similar to that for activation of L-type Ca channel ionic current, over a broad voltage range. The current associated with Q_{off} decays monoexponentially and more slowly than ionic current. Similar charge movements are found in guinea pig tracheal myocytes, which lack Na channels and T-type Ca channels. The kinetic and pharmacological properties of Q_{on} and Q_{off} indicate that they reflect gating currents associated with L-type Ca channels. ω-Aga-IIIA has no effect on gating currents when ionic current is eliminated by stepping to the reversal potential for Ca or by Cd block. Gating currents constitute a significant component of total current when physiological concentrations of Ca are present and they obscure the activation and deactivation of L-type Ca channels. By using ω-Aga-IIIA, we resolve the entire time course of L-type Ca channel ionic and gating currents. We also show that L- and T-type Ca channel ionic currents can be accurately quantified by tail current analysis once gating currents are taken into account.

INTRODUCTION

The spider toxin ω-Aga-IIIA blocks currents through L-type Ca channels in cardiac myocytes with no effect on T-type Ca channels (Mintz, Venema, Adams, and Bean, 1991; Cohen, Ertel, Smith, Venema, Adams, and Leibowitz, 1992a). Our earlier study

with this toxin indicated a need to reevaluate the use of tail current analysis to quantify L-type Ca currents. Tail currents reflect the closing of ion channels (deactivation) and they are observed when a voltage-clamped membrane is repolarized after a depolarizing pulse that activates channels. L-type Ca channels deactivate more rapidly than T-type Ca channels (Cota, 1986; Matteson and Armstrong, 1986; Carbone and Lux, 1987; Cohen, McCarthy, Barrett, and Rasmussen, 1988; Hiriart and Matteson, 1988; Kostyuk and Shirokov, 1989; McCarthy and Cohen, 1989; Cohen, Spires, and Van Skiver, 1992b). We and others have interpreted the slowly and the rapidly decaying components of Ca channel tail current as being entirely due to ionic current through T-type and L-type Ca channels, respectively. However, in guinea pig atrial myocytes, a substantial fraction of the rapidly decaying component is resistant to block by ω-Aga-IIIA (Cohen et al., 1992a). This result suggests that block of L-type Ca channels by ω-Aga-IIIA is incomplete, and/or that intramembrane charge movements can constitute a significant fraction of the tail currents in atrial cells, as shown earlier for ventricular cells (Hadley and Lederer, 1991). We find that the toxin-resistant rapidly decaying tail current is entirely due to intramembrane charge movements. We present evidence that these charge movements represent gating currents associated with L-type Ca channels.

Gating currents are asymmetric intramembrane charge movements that arise when charged components of voltage-gated ion channels move in response to a change in transmembrane voltage (Armstrong, 1981; Bezanilla, 1985). Gating current measurements can reflect the time and voltage dependences of transitions between closed states of ion channels and thereby complement studies of the kinetics of ionic currents through open channels. Gating currents associated with Na channels are particularly well documented. Two factors have facilitated these studies: (a) some neurons and myocytes have a high density of Na channels and few other channels that open at similar rates and voltages; and (b) several toxins, such as tetrodotoxin, block ionic current through Na channels with little or no effect on the voltage dependence of channel gating. Until now, such favorable conditions were not available to study gating currents associated with Ca channels. However, several recent studies have indicated that ventricular myocytes possess a large component of dihydropyridine (DHP)-sensitive intramembrane charge movement, presumably arising from the gating of L-type Ca channels (Field, Hill, and Lamb, 1988; Bean and Rios, 1989; Hadley and Lederer, 1991; Josephson and Sperelakis, 1992; Shirokov, Levis, Shirokova, and Rios, 1992). These studies have relied on transition metals such as Cd, Co, and/or La to suppress ionic currents because they lacked high-affinity blockers of Ca channel ionic current. Unfortunately, block of L-type Ca channels by these cations is very voltage dependent (Lansman, Hess, and Tsien, 1986), such that high concentrations are required to isolate the gating current associated with channel deactivation. Such concentrations could affect Ca channel gating currents in the same way that transition metals modify Na channel gating currents (Armstrong and Cota, 1990; Sheets and Hanck, 1992) and DHP-sensitive displacement currents in skeletal muscle (Rios and Pizarro, 1991). By using ω-Aga-IIIA, one can measure ionic and gating currents under nearly identical conditions because the toxin blocks ionic current through L-type Ca channels and has no effect on the associated gating currents.

MATERIALS AND METHODS

Cell Preparations

Single guinea pig atrial myocytes were prepared from male Duncan-Hartley guinea pigs as described previously (Mitra and Morad, 1985; Cohen et al., 1992b). Tracheal myocytes were isolated by adapting protocols used for vascular smooth muscle cells (Warshaw, Szarek, Hubbard, and Evans, 1986; Clapp and Gurney, 1991). A cleaned, intact trachea was incubated on ice for 30 min in dissociation solution (in mM): NaCl 135, KCl 5.4, $CaCl_2$ 0.2, $MgCl_2$ 1, NaH_2PO_4 0.33, HEPES 10, pH 7.3 with NaOH, containing 40 U/ml papain. The papain was activated by warming to 37°C in the presence of 2 mM dithiothreitol and the tissue was digested for 25 min. The trachea was washed several times with dissociation solution, suspended in the same solution containing 300 U/ml collagenase (Worthington type II) and 190 U/ml elastase (Sigma type IV) and the solution was circulated through the lumen of the trachea for 20 min. Digestion was terminated by washing with dissociation solution containing 0.5 mg/ml soybean trypsin inhibitor and 2 mg/ml bovine serum albumin. The trachea was washed with relaxing solution (in mM): K-glutamate 140, $MgCl_2$ 5, EGTA 1, HEPES 10, dextrose 10, pH 7.4 with KOH, supplemented with 60 U/ml DNase II (Sigma type V). The tissue was then cut into small pieces and triturated, and the dissociated cells were washed repeatedly with sterile relaxing solution. They were then placed in Medium 199 at 37°C, and 100 µM dibutyryl-cAMP and 100 µM 3-isobutyl, 1-methylxanthine were added to facilitate relaxation. The cells were placed in media for at least 1 h before use and were used within 12 h of dissociation.

Whole-Cell Voltage Clamp Measurements

Cells were voltage-clamped as described previously (Cohen et al., 1992b), using the whole-cell configuration of the patch clamp technique at room temperature (20–25°C) (Hamill, Marty, Neher, Sakmann, and Sigworth, 1981). Early experiments used an Axopatch 1A amplifier (Axon Instruments, Inc., Burlingame, CA) and later experiments used a model 3900 amplifier (Dagan Corp., Minneapolis, MN). Membrane current was low-pass filtered using a four-pole Bessel filter with a cutoff frequency (f_c, -3 dB) of 5 kHz and digitized at 40 kHz, unless otherwise indicated. Linear leak and capacity currents were subtracted digitally by scaling the average response to 16 test pulses from -100 to -140 mV. These responses were unaffected by 60 nM ω-Aga-IIIA and/or 4 µM felodipine. The linear capacitance of cells used in these studies ranged from 15 to 35 pF. Zero Ca current was defined as the current at the holding voltage and this level is indicated by a dashed line where appropriate. Tail currents were fit by one or the sum of two exponentials plus a constant using the Levenberg-Marquardt nonlinear curve fitting algorithm (Press, Flannery, Teukolsky, and Vetterling, 1986). When fitting a family of tail current records spanning a wide range of current amplitudes, e.g., current–voltage relationships, a multistep procedure was used. First, in the case of a double exponential, each record was fit with the two time constants and three amplitudes free to vary, so as to obtain the best fit for each record. Then, for each of the two time constants, the mean was calculated for the four or five records with the largest amplitudes. Finally, each record was fit a second time with the time constants fixed to these calculated values. The reported tail current amplitudes are those obtained in the second fit. A similar procedure was used for single exponential fits.

Changes in membrane voltage were complete within 200–250 µs (atria) or 550–650 µs (trachea) after a change in command voltage and data collected during this interval were excluded from analysis and display, unless otherwise indicated. The reported tail current amplitudes represent the magnitude of the fitted exponentials at the end of this period. Intramembrane charge movement was calculated as the time integral over 5 ms of the toxin-insensitive, felodipine-sensitive current. Where specified, data were fit by a two-state

Boltzmann distribution (I/I_{max} = {1 + exp [($V_{1/2}$ − V)/k]]$^{-1}$), where I_{max} is the maximum amplitude, $V_{1/2}$ is the midpoint potential, and k is the slope factor. Means are given with the standard error of the mean (SEM).

We were concerned about possible errors in the quantification of currents immediately after a step in membrane voltage. The results shown in Figs. 2 and 4 (q.v.) allow us to estimate the amount of ionic tail current that was lost during the blanking period. Fig. 2 D shows that the maximal amplitude of the ionic tail current at −50 mV was on average 340% of the current at +20 mV. The Boltzmann distribution for activation of ionic tail current has a midpoint at 17.4 mV and a slope factor of 11.7 mV, so the amplitude of the tail current after a step to +20 mV is on average 340%/{1 + exp((17.4−20)/11.7)} ≈ 190% of the current during the step to +20 mV. The ideal change in amplitude can be estimated from single-channel conductance measurements. The most appropriate available data are for cell-attached patches with 10 mM Ca as the charge carrier, where the single channel current at −50 mV is ≈ 300% of the current at +20 mV (Yue and Marban, 1990). Hence, we measure ≈ (190/300) × 100% ≈ 63% of the possible tail current. The percent loss of ionic tail current is nearly constant when channel opening is changed by toxin block or channel inactivation, so that we are able to adequately quantify tail currents through L-type Ca channels (see Fig. 2 and Discussion). The corresponding charge movement (Q_{off}) and its associated transient current ($I_{g,off}$) have slower kinetics than the tail currents, so quantification of Q_{off} and $I_{g,off}$ is also adequate. Q_{off} and the charge movement at the beginning of a test depolarization (Q_{on}) are equal in magnitude (see Figs. 4, 5, and 7), suggesting that Q_{on} and its associated transient current ($I_{g,on}$) are also adequately separated from the linear capacity current. It is possible that a very rapidly decaying component of $I_{g,on}$ is underestimated at very positive test potentials, but the total charge associated with this component is presumably small. Faster voltage changes could be achieved with the Dagan model 3900 amplifier, but the charge movements were indistinguishable from those observed using the Axopatch 1A. Several experiments were conducted with reduced gain to eliminate saturation of the analog-to-digital converter and, despite the introduction of "bit noise," the charge movements were similar to those recorded at higher gain.

Solutions and Drugs

ω-Aga-IIIA was isolated from the venom of *Agelenopsis aperta* by ion exchange and reverse phase liquid chromatography (Ertel, Warren, Adams, Griffin, Cohen, and Smith 1994). The 1,4-dihydropyridine felodipine, a more potent congener of nifedipine (Nyborg and Mulvany, 1984), was synthesized at Merck. A 1 mM stock solution in ethanol was diluted to achieve the desired final concentration.

The external (bath) and internal (pipette) solutions for electrophysiological experiments were designed to minimize currents through Na and K channels. The internal solution contained (in mM): Cs-glutamate 107, CsCl 20, tetrabutylammonium-Cl 1, 1,2-bis(2-aminophenoxy)-ethane-N,N,N',N'-tetraacetic acid (BAPTA) 11, CaCl$_2$ 0.9, MgCl$_2$ 1, HEPES 20, Mg-ATP 5, Li$_2$-GTP 0.1, pH 7.2 with CsOH. The bath solution contained (in mM): tetraethylammonium (TEA)-Cl 157, CaCl$_2$ 5, MgCl$_2$ 0.5, HEPES 10, pH 7.5 with CsOH, 0.05% fatty-acid free bovine serum albumin. Solutions were pressurized with 100% O$_2$.

RESULTS

ω-Aga-IIIA defines two components of rapidly decaying Ca channel tail current in atrial myocytes (Fig. 1). Currents are shown for a holding potential of −50 mV, a test pulse potential of +20 mV and a repolarization potential of −50 mV, so that the two voltage steps are symmetrical. Only L-type Ca channels are available to conduct because Na channels, T-type Ca channels, and K channels are blocked or inactivated.

Currents were recorded without drug, in 60 nM ω-Aga-IIIA and in toxin plus 4 μM felodipine (Fig. 1, A–C, respectively). In the control record, the depolarization causes a rapidly decaying outward transient followed by an inward current; after repolarization, there is a large inward tail current. The current recorded with 60 nM ω-Aga-IIIA shows that the toxin has no effect on the outward transient, blocks the inward current during the test pulse (revealing a small outward current), and reduces the rapidly decaying tail current by ≈ 70%. The toxin-insensitive rapidly decaying tail current is present when all L-type Ca channel ionic current is blocked during the test pulse to
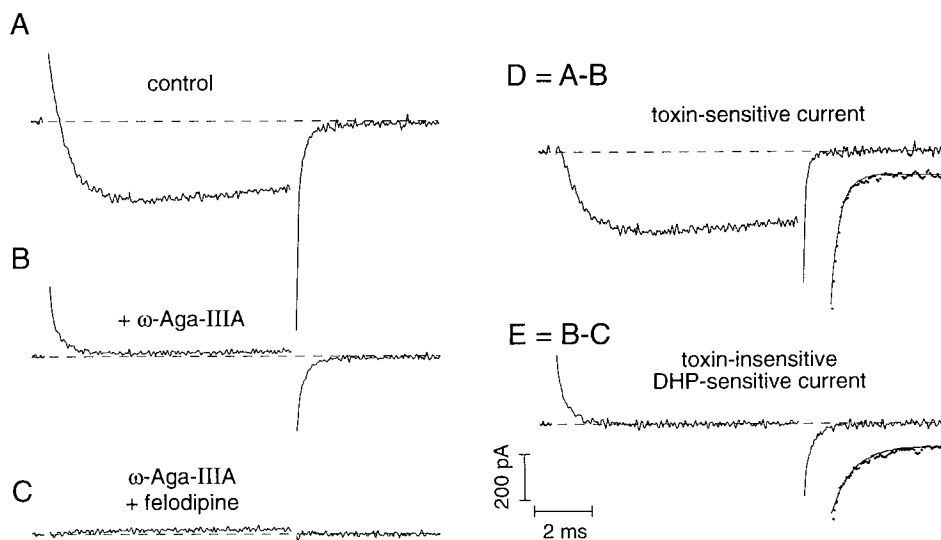

FIGURE 1. ω-Aga-IIIA and felodipine reveal two pharmacologically distinct currents. (*A*) Control current induced by a test pulse to +20 mV from a holding voltage of −50 mV (repolarization to −50 mV). Same voltage protocol (*B*) in the presence of 60 nM ω-Aga-IIIA and (*C*) in the presence of both 60 nM ω-Aga-IIIA and 4 μM felodipine. (*D*) The toxin-sensitive current calculated by subtracting the record in toxin (*B*) from that in control (*A*). (*E*) The toxin-insensitive, DHP-sensitive current calculated by subtracting the record in toxin plus felodipine (*C*) from that in toxin alone (*B*). The tail currents are fit with single exponentials yielding time constants of 0.13 ms for the toxin-sensitive tail (*D*) and 0.30 ms for the toxin-insensitive, DHP-sensitive tail (*E*). In the insets of *D* and *E*, the first 1.5 ms of the tail currents are expanded in the time axis, shifted downward slightly, and shown with the corresponding exponential fit. Blanking interval, 200 μs; cell capacitance, 24 pF.

+20 mV, and it is about the same size as the outward current transient at the beginning of the pulse. The addition of 4 μM felodipine blocks all remaining transient currents. For the toxin-sensitive current (Fig. 1 *D*), the tail current is fit by a single exponential with a time constant of decay (τ) equal to 0.13 ms (*inset*). For the toxin-insensitive, DHP-sensitive current (Fig. 1 *E*), the tail current is also well fit by a single exponential, but the time constant of decay is slower than for the toxin-sensitive component (τ = 0.30 ms). We consistently found that the toxin-sensitive tail current decays more rapidly than the toxin-insensitive tail current; the average ratio

of time constants is 2.24 ± 0.10 (n = 18). This ratio may be an underestimate because the time constant of decay of the toxin-sensitive component could be limited by the bandwidth of our recordings. The differing rates of decay suggest that the toxin-sensitive and toxin-insensitive tail currents arise from different sources.

In earlier studies, including some from this laboratory, the amplitude of the rapidly decaying tail current was taken as a measure of the instantaneous conductance of L-type Ca channels. The results shown in Fig. 1 suggest either that in atrial myocytes, a substantial fraction of the rapidly decaying tail current is not due to ionic current through L-type Ca channels or that block of L-type Ca channels by ω-Aga-IIIA is voltage dependent, such that block is relieved upon repolarization of the membrane. Although such voltage-dependent block occurs with Cd and some other transition metals, the following figures show that ω-Aga-IIIA blocks all ionic current through L-type Ca channels with high affinity and that the toxin-resistant tail current is entirely due to intramembrane charge movements.

The instantaneous conductance of L-type Ca channels is proportional to the toxin-sensitive tail current (Fig. 2). Fig. 2 A shows that the toxin-insensitive tail current remains unaffected even at very high toxin concentrations. The amplitude of the rapidly decaying tail current is plotted as a function of test potential (V_t). 1.5 nM ω-Aga-IIIA produces more than half-maximal block. For large depolarizations, 80 nM ω-Aga-IIIA blocks about two-thirds of the total current although it appears less potent for smaller depolarizations. 240 nM ω-Aga-IIIA produces no additional block, indicating that a maximal effect has been achieved. Hence, it is unlikely that the toxin-resistant tail current represents incomplete block of ionic current through L-type Ca channels. Finally, 1 μM felodipine suppresses the toxin-resistant rapidly decaying tail current, as in Fig. 1.

Fig. 2 B shows that the dose-response curve for block of L-type Ca channels based on measurements of current during a test pulse to +20 mV (●, $ED_{50} \approx 0.38$ nM) closely coincides with the curve based on measurements of toxin-sensitive tail currents (□, $ED_{50} \approx 0.35$ nM). The agreement between these curves indicates that our measurements of toxin-sensitive tail current accurately assay block of L-type Ca channels. In Fig. 2 C, we compare the magnitudes of the toxin-sensitive tail currents measured after test pulses to +20 mV of various durations with the amplitude of the toxin-sensitive Ca current during a single long pulse: they are proportional at all times. Thus, identical rates of inactivation are inferred from the toxin-sensitive current measured during a long test pulse and from the envelope of tail current measurements. In Fig. 2 D, we show that, for 18 myocytes, the amplitude of the Boltzmann distribution of the toxin-sensitive tail currents is proportional to that of the Ca current at the end of a 10-ms test pulse to +20 mV.

The time constant of decay of the toxin-sensitive tail current is not much slower than the settling time of the membrane voltage after a voltage step. Therefore, this settling time is likely to introduce an error in the measurement of the percentage of tail current blocked by toxin. Nevertheless, the results presented in Fig. 2 indicate that changes in the amplitude of the toxin-sensitive tail currents accurately reflect changes in the instantaneous conductance of L-type Ca channels.

We have shown that felodipine suppresses the toxin-insensitive tail current. Since DHPs suppress some asymmetric charge movement in myocardial cells (Field et al.,
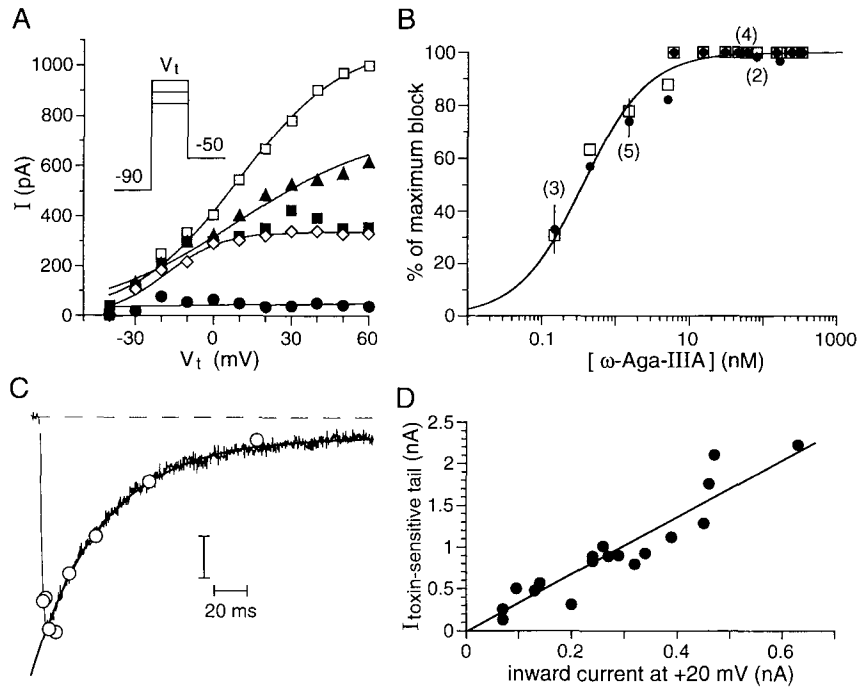
FIGURE 2. The magnitude of the toxin-sensitive rapidly decaying tail current provides an accurate representation of the instantaneous conductance of L-type Ca channels. (*A*) Maximally effective concentrations of ω-Aga-IIIA fail to block completely the rapidly decaying tail current. In this experiment, the holding voltage was −90 mV so that currents through both L- and T-type Ca channels were present. The amplitude of the rapidly decaying component was calculated from biexponential fits of the tail currents and is plotted as a function of test pulse voltage (V_t). □, control; ▲, 1.5 nM; ◇, 80 nM; ■, 240 nM ω-Aga-IIIA; ●, 240 nM toxin plus 1 μM felodipine. The fits by two-state Boltzmann distributions were: □, $V_{1/2}$ = 8.8 mV, k = 19.0 mV; ▲, $V_{1/2}$ = −3.4 mV, k = 18.6 mV; ◇, ■, $V_{1/2}$ = −19.3 mV, k = 10.6 mV. Test pulse duration, 10 ms; blanking interval, 250 μs; time constants of tail current decay, 0.23 ms and 3.10 ms; cell capacitance, 25 pF. (*B*) Dose-response curves for block of L-type Ca channels based on measurements of either current at the end of a test pulse to +20 mV (●) or the amplitude of the Boltzmann distribution of the tail currents at −50 mV (□). Test pulse, 10 ms; holding voltage, −90 mV. The data indicate the percentage of the effect produced by ≥ 30 nM ω-Aga-IIIA; the maximal effects were 59 ± 4% block of the tail current and 90 ± 2% block of the current during the test pulse (n = 9). The data sets are fit by 1:1 binding curves with dissociation constants of 0.35 nM and 0.38 nM, respectively (both curves are drawn). The numbers in parenthesis indicate the number of measurements performed for a given toxin concentration, if more than one. (*C*) Comparison of the toxin-sensitive current during a test pulse to +20 mV and the toxin-sensitive rapidly decaying tail current, from a holding voltage of −90 mV. The current trace is the current sensitive to 60 nM ω-Aga-IIIA during a "long" 200-ms test pulse (filter, 2 kHz; sampling, 4 kHz; blanking interval, 500 μs). ○, magnitude of the toxin-sensitive tail current at −50 mV measured after test pulses lasting 3, 4, 6, 10, 18, 34, 66, and 130 ms (blanking interval, 250 μs; time constant, 250 μs). (*Vertical calibration bar*) 75 pA for the tail currents, 63 pA for the current trace. Both the current trace and the envelope of tails were well fit by a monoexponential decay with a time constant of 42 ms. Cell capacitance, 23 pF. (*D*) For 18 myocytes, the amplitude of the Boltzmann distribution of the tail currents at −50 mV is plotted versus the amplitude of the inward Ca current at the end of a test pulse to +20 mV from a holding voltage of −50 mV. The data were fit with a slope of 3.4 (r = 0.93). Test pulse, 10 ms; cell capacitances, 15–35 pF.

1988; Hadley and Lederer, 1991), our working hypothesis was that ω-Aga-IIIA blocks ionic current through L-type Ca channels, but not the associated gating current. Figs. 3 and 4 show that the toxin-insensitive tail current ($I_{g,off}$) appears to be a single component of intramembrane charge movement. Fig. 3 shows the combined effect of
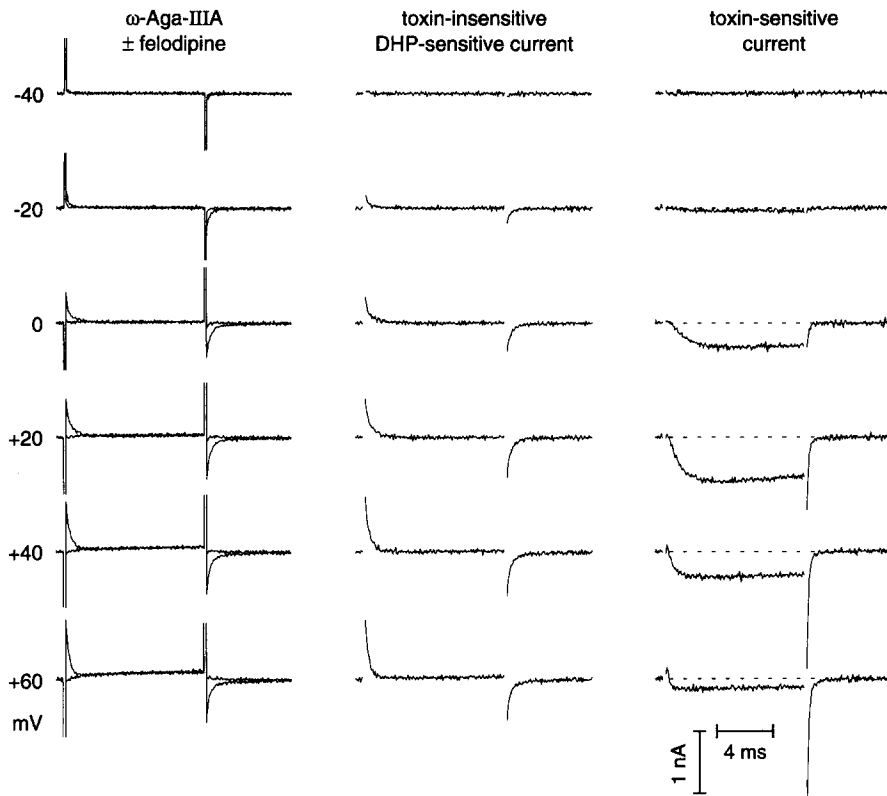

FIGURE 3. Time courses of the toxin-sensitive and the toxin-insensitive, DHP-sensitive currents over a broad range of test potentials. Holding and repolarization voltages were −50 mV. The left column shows superimposed current records in 60 nM ω-Aga-IIIA with and without 4 μM felodipine. These current records are not "blanked" during the settling time of the voltage clamp amplifier but, at the scale used, the full magnitude of the current during the capacity transients is not shown (saturation occurred at ≈3.5 nA). The middle column shows the felodipine-sensitive current corresponding to each current pair shown at left, with 200 μs blanked at the start of voltage steps. The right column shows the current blocked by ω-Aga-IIIA before the addition of felodipine, with 200 μs blanked at the start of voltage steps. Cell capacitance, 24 pF.

ω-Aga-IIIA and felodipine, as in Fig. 1, over a broad range of test potentials. The left column shows superimposed current records in 60 nM ω-Aga-IIIA with and without 4 μM felodipine. These current records are not "blanked" during the settling time of the voltage clamp amplifier and saturation of the analog to digital converter is

apparent at the most positive test potentials. The middle column shows the felodipine-sensitive current corresponding to each pair of currents shown at the left, with 200 μs blanked at the start of the voltage steps. The right column shows the current blocked by ω-Aga-IIIA before the addition of felodipine. The toxin completely blocks the inward current during the test pulse at all test potentials, whereas it does not affect the outward transient ($I_{g,on}$). The toxin-insensitive tail current activates at more negative potentials than the toxin-sensitive tail current (this is seen most clearly in the records for $V_t = -20$ mV), so that most of the total tail current is toxin insensitive for $V_t < +20$ mV.

Fig. 4 shows the magnitude of the charge movements and the toxin-sensitive tail current as functions of test potential, calculated from the data in Fig. 3. Charge movement is the time integral of the felodipine-sensitive currents at the beginning of the test pulse (Q_{on}) and just after repolarization (Q_{off}). Q_{on} and Q_{off} are of equal magnitude and both saturate as the test pulse potential increases. This indicates that
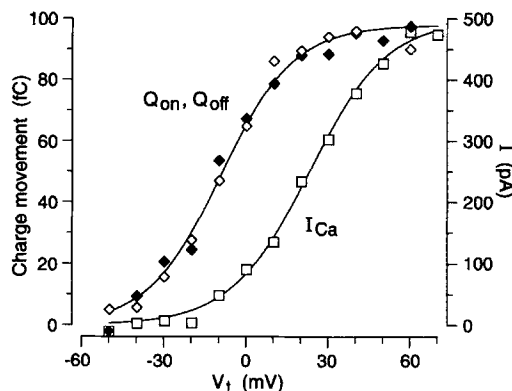

FIGURE 4. Voltage dependence of Q_{on}, Q_{off}, and L-type Ca channel ionic current. The ionic current (□) was calculated for each test pulse voltage by fitting a single exponential to the tail current sensitive to 60 nM ω-Aga-IIIA. The time constant of decay was 0.13 ms. Q_{on} (◇) and Q_{off} (◆) were calculated as described in Materials and Methods. The parameters defining the Boltzmann distributions were: $V_{1/2} = 23.0$ mV, $k = 14.2$ mV for the ionic current, and $V_{1/2} = -9.2$ mV, $k = 13.2$ mV for Q_{on} and Q_{off}. Holding and repolarization potentials, -50 mV; cell capacitance, 24 pF.

the transient currents in the presence of ω-Aga-IIIA reflect intramembrane charge movements. The solid curves are fits by a two-state Boltzmann distribution to the data for Ca ionic current and the magnitude of Q_{off}. A similar voltage dependence of activation was observed in 16 experiments conducted with a maximally effective concentration of ω-Aga-IIIA. For a holding potential of -50 mV, the distribution describing the intramembrane charge movement had an average magnitude of 3.9 ± 0.4 nC/μF, a midpoint of -16.7 ± 2.2 mV and a slope factor of 10.7 ± 0.7 mV. The toxin-sensitive tail current had an amplitude of 730 ± 130 pA, a midpoint of 17.4 ± 1.2 mV and a slope factor of 11.7 ± 0.5 mV. When channels are maximally activated, $I_{g,off}$ represents a substantial fraction (16% ± 2%) of the total rapidly decaying tail current, as previously found for guinea pig ventricular myocytes (Hadley and Lederer, 1991). In addition, the midpoint for intramembrane charge movement is 34 mV more negative than that for the activation of ionic current. Thus, $I_{g,off}$

constitutes an even greater proportion of total tail current for test potentials that cause sub-maximal activation.

The kinetics of the DHP-sensitive charge movement is consistent with gating current associated with L-type Ca channels (Fig. 5). Each panel of Fig. 5 A shows the toxin-insensitive (top) and toxin-sensitive (bottom) currents measured immediately after a test pulse to the indicated voltage. To fit the records, we used m^3 activation
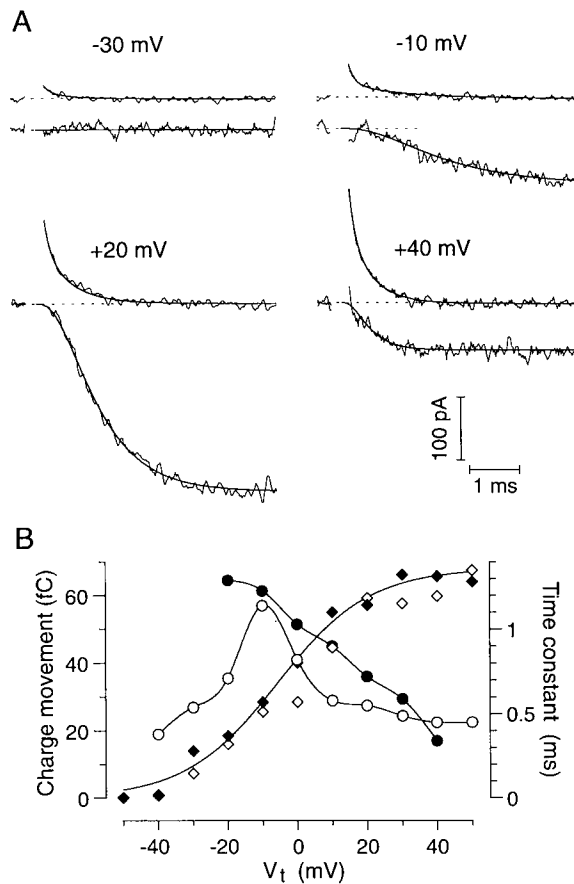

FIGURE 5. The rate of activation of ionic current through L-type Ca channels is consistent with the rate of decay of $I_{g,on}$. (A) ω-Aga-IIIA-sensitive current and felodipine-sensitive, toxin-insensitive on-transients from a holding potential of -50 mV to the indicated test potentials. The dashed lines indicate the zero-current level; the current records are offset slightly for $V_t = -30$ and -10 mV. The ionic current records (lower trace in each subpanel) were fit with a third order equation $\{I(t)=I_{max}\times[1-\exp(-t/\tau)]^3\}$, whereas the outward transients (upper traces) were fit with the sum of two exponentials plus a constant (fast time constant was fixed at 120 μs, slow time constant was free). ω-AgaIIIA, 60 nM; felodipine, 1 μM. (B) The time constant of activation of the ionic current ($\bullet$), the slow time constant of decay of $I_{g,on}$ ($\bigcirc$), and the magnitudes of Q_{on} and Q_{off} ($\Diamond$, $\blacklozenge$) are plotted as functions of test pulse voltage. The parameters defining the Boltzmann distribution were: $V_{1/2} = -6.7$ mV, $k = 13.0$ mV. Blanking interval, 350 μs; cell capacitance, 17 pF.

kinetics for the toxin-sensitive current and the sum of two exponentials for the toxin-insensitive current. Although the decay of $I_{g,on}$ can be reasonably well fit by a single exponential at very positive test potentials, it clearly requires at least two exponentials for weaker depolarizations. In Fig. 5 B, we have plotted the time constant of the slowly decaying component of $I_{g,on}$ ($\bigcirc$), the time constant describing m^3 activation of ionic current ($\bullet$), and the magnitudes of Q_{on} and Q_{off} ($\Diamond$, $\blacklozenge$) as

functions of test pulse voltage. There are three important points in this figure. First, the outward transients are finished at the time of peak inward toxin-sensitive current, as expected if the gating currents are associated with opening the channel that conducts the ionic current. Second, the time constant of the slowly decaying component of $I_{g,on}$ has a bimodal dependence on V_t and is slowest near the midpoint of the curve describing activation of Q_{on} and Q_{off}. Third, the magnitude and the voltage dependence of the time constant describing the activation of ionic current are similar to those of the slow time constant of $I_{g,on}$. Although the two time constants are essentially equal for $V_t \geq +40$ mV ($\tau \approx 0.4$ ms), the activation of ionic current is slightly slower than the decay of $I_{g,on}$ for V_t between -20 and $+30$ mV. A similar result was obtained in two other experiments. In the Hodgkin-Huxley type model that we use, this difference could arise if one of the three consecutive transitions between preactivated states were slightly slower than the other two. The time course of $I_{g,on}$ is therefore consistent with a gating current arising from a series of transitions between closed states of L-type Ca channels. Similarly, the time course of $I_{g,off}$ is consistent with L-type Ca channel gating current because it decays more slowly than ionic tail current through L-type Ca channels (Fig. 1).

The magnitude of the gating charge movement in our studies ($Q_{max} = 3.9 \pm 0.4$ nC/μF) is similar to that reported in previous studies of myocardial L-type Ca channel gating currents (Field et al., 1988; Hadley and Lederer, 1989; Shirokov et al., 1992). Also, as previously observed (Bean and Rios, 1989; Hadley and Lederer, 1991), Q_{max} is not proportional to the amplitude of L-type Ca channel ionic current among different cells ($r < 0.25$, not shown). This result may arise from unequal amounts of run-down of the ionic current among the different cells.

The DHP-sensitive charge movement that we have characterized in atrial myocytes could include intramembrane charge movements from sources other than L-type Ca channels. The possible charge movements of greatest concern are those associated with Na channels, T-type Ca channels, or the sensor for intracellular Ca release. Guinea pig tracheal myocytes have a fairly high density of L-type Ca channels, but none of the likely contaminating charge movements (data not shown). Nonetheless, the toxin-insensitive tail current in this airway smooth muscle is very similar to that found in atrial myocytes (Fig. 6). The protocol used in this experiment is identical to that used for Fig. 4, except that the holding potential was -90 mV. Fig. 6A shows superimposed current records for test potentials of 0 and $+20$ mV with and without a maximally effective concentration of ω-Aga-IIIA. The effects of toxin are very similar to those observed with atrial cells when the holding potential is -50 mV: the toxin has little or no effect on the outward transient but it blocks the inward current during the test pulse as well as a component of tail current that decays more rapidly than the toxin-insensitive tail current. Tracheal myocytes are less suited to experiments that require rapid voltage steps because they are long and very thin (diameter ≈ 5 μm). The experiment shown is one of two in which we observed robust L-type Ca channel currents and a reasonably brief capacity transient (settling time of ≈ 600 μs). In this cell, the voltage dependences of activation of Q_{on}, Q_{off}, and the toxin-sensitive tail current (Fig. 6B) were all similar to those found in atrial cells (Fig. 4). In other experiments, we found that the tail current is completely blocked by micromolar felodipine (data not shown). Since airway smooth muscle has L-type Ca channels that

are nearly identical to those in cardiac muscle but lacks Na channels, T-type Ca channels, and the sensor for intracellular Ca release, it is likely that Q_{on} and Q_{off} reflect only L-type Ca channel gating current.

The evidence presented thus far argues that the toxin-insensitive, DHP-sensitive current is gating current associated with L-type Ca channels. For studies of gating currents, it is ideal to have a toxin that blocks ionic current through the target channel with high affinity, but has no effect on the gating current. To show that ω-Aga-IIIA does not modify $I_{g,on}$, we eliminated ionic current during a test pulse with two techniques other than toxin application. In Fig. 7 A, we stepped the membrane voltage from −50 to +70 mV, which is near the reversal potential for Ca. In this case,
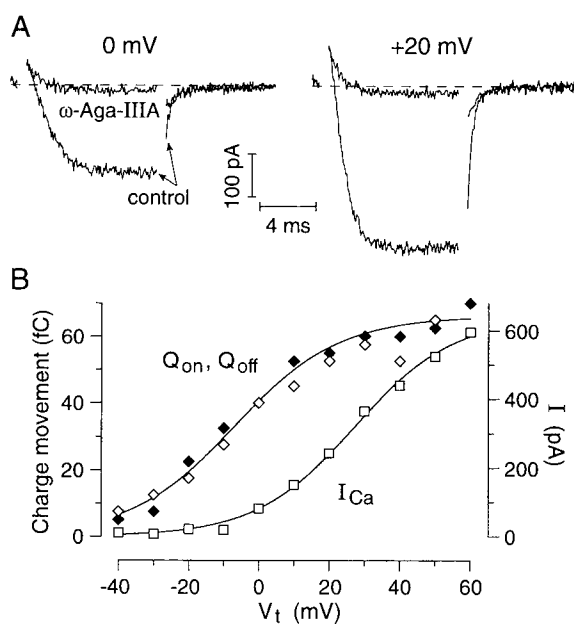

FIGURE 6. ω-Aga-IIIA isolates gating currents associated with L-type Ca channels in guinea pig tracheal myocytes. (A) Current records in control and in 175 nM ω-Aga-IIIA, for a holding voltage of −90 mV, a 10-ms test pulse to 0 mV or +20 mV, and a repolarization to −50 mV. (B) Voltage dependence of Q_{on}, Q_{off}, and L-type Ca channel ionic tail current. The ionic tail current (□) was calculated for each test pulse voltage by fitting a single exponential to the ω-Aga-IIIA-sensitive tail current. The time constant was 0.25 ms. Q_{on} (◇) and Q_{off} (◆) were calculated as described in Materials and Methods except that an integration interval of 2.5 ms was used. The parameters defining the Boltzmann distributions were: $V_{1/2}$ = 27.2 mV, k = 14.1 mV for the ionic current, and $V_{1/2}$ = −8.1 mV, k = 14.3 mV for Q_{on} and Q_{off}. Blanking interval, 600 μs; cell capacitance, 31 pF.

the control current during the test pulse is almost entirely L-type Ca channel gating current. 60 nM ω-Aga-IIIA had little or no effect on the gating current, although it revealed that the control current during the test pulse was composed of a small inward Ca current and a small contaminating outward current. The gating current was completely eliminated by 4 μM felodipine. Similar effects of ω-Aga-IIIA and felodipine are shown in Fig. 3, where all of the toxin-sensitive currents in the right column lack a transient at the beginning of the test pulse.

We also isolated gating current before adding toxin by blocking L-type Ca channels with Cd (Fig. 7, B and C). Fig. 7 B shows the effects of the successive applications of 100 μM Cd, 60 nM ω-Aga-IIIA, and 1 μM felodipine. Cd has little or no effect on the

outward transient at the beginning of the test pulse, blocks the inward current during the test pulse, and partially blocks the tail current. ω-Aga-IIIA blocks the tail current further and has no effect on the current during the test pulse. Addition of felodipine suppresses the remaining transient currents. Fig. 7 C shows the charge movements calculated for the current transients in Cd alone or in Cd plus ω-Aga-IIIA. As in Fig. 4, Q_{on} and Q_{off} are of equal magnitude at all voltages in ω-Aga-IIIA. In addition, Q_{on} is nearly identical with and without ω-Aga-IIIA, confirming that the toxin does not modify gating current. Because 100 μM Cd does not completely block L-type Ca
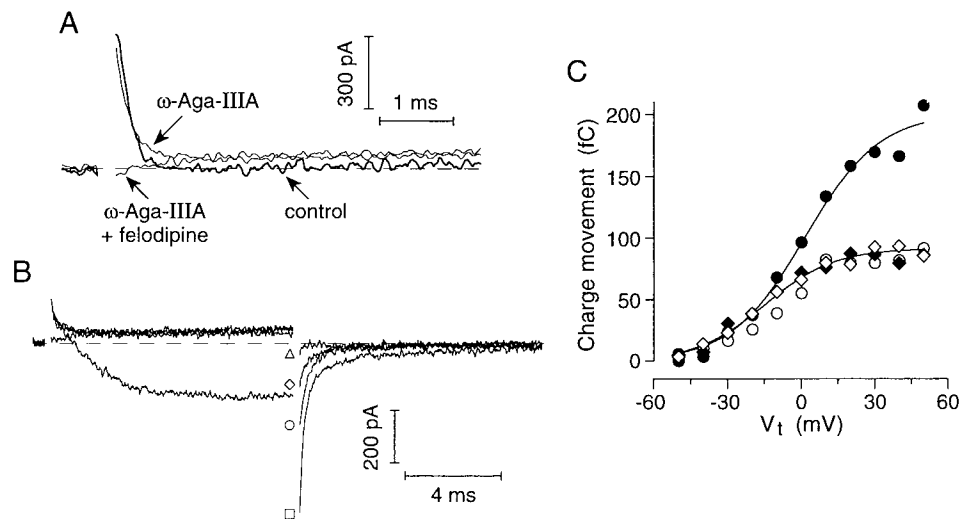

FIGURE 7. ω-Aga-IIIA does not affect Q_{on}. (A) Q_{on} isolated by stepping near the reversal potential for I_{Ca}. Current records for test pulses to +70 mV from a holding potential of −50 mV; control (*thicker trace*), in 60 nM ω-Aga-IIIA, and in toxin plus 4 μM felodipine. Blanking interval, 200 μs; cell capacitance, 24 pF. (B) Q_{on} isolated by blocking I_{Ca} during the test pulse with Cd. Current records for test pulses to +20 mV from a holding potential of −50 mV (repolarization potential, −50 mV). □, control; ○, 100 μM Cd; ◇, Cd plus 60 nM ω-Aga-IIIA; and △, Cd plus toxin plus 1 μM felodipine (trace with no outward transient at start of test pulse). (C) Q_{on} and Q_{off} calculated as described in Materials and Methods and plotted versus test pulse voltage, for the same experiment as in B. ○ and ●, Q_{on} and Q_{off} in 100 μM Cd; ◇ and ◆, Q_{on} and Q_{off} in Cd plus toxin. The parameters defining the Boltzmann distributions were: ○, $V_{1/2}$ = −11.1 mV, k = 12.5 mV (not shown); ●, $V_{1/2}$ = 1.5 mV, k = 15.2 mV; ◇ and ◆, $V_{1/2}$ = −14.9 mV, k = 14.2 mV. Blanking interval, 250 μs; cell capacitance, 24 pF.

channel ionic currents, especially tail currents, Q_{off} is of greater magnitude than Q_{on} in Cd alone. A similar voltage dependence of Ca channel block by Cd has been reported in invertebrate neurons and in ventricular myocytes (Byerly, Chase, and Stimers, 1984; Lansman et al., 1986; Chow, 1991).

Previous studies of DHP-sensitive gating currents in myocardial cells used transition metals to block ionic Ca channel currents at all voltages. Our results indicate that 100 μM Cd is adequate to isolate Q_{on} (but not Q_{off}) and that the gating current so obtained is similar to that isolated with ω-Aga-IIIA. However, much higher concen-

trations of Cd were usually used in previous studies to isolate both Q_{on} and Q_{off} and this causes modification of gating currents in our studies. Charge movement was measured using the same protocol shown in Fig. 4, except that Cd was added after ω-Aga-IIIA. 2 mM Cd reduced charge movement for a test pulse to +20 mV by 13 ± 4% ($n = 7$; data not shown).

T-type Ca channels inactivate when cells are held at depolarized potentials (≥ -50 mV) and therefore contribute negligible current in most of the experiments discussed thus far. However, these channels are available to open when cells are held at normal
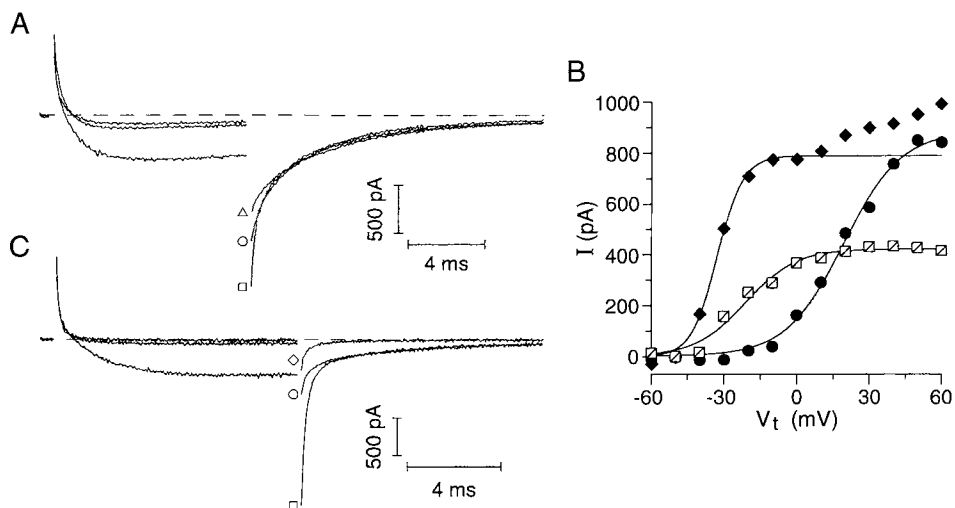

FIGURE 8. ω-Aga-IIIA, Cd, and felodipine define three components of tail current. (*A*) Current records for a holding voltage of −90 mV, a test pulse to +20 mV, and a repolarization to −50 mV: □, control (*lower trace* during the test pulse); ○, 80 nM ω-Aga-IIIA (*middle trace*); and △, 240 nM toxin plus 1 μM felodipine (*upper trace*). Blanking interval, 250 μs; cell capacitance, 25 pF. (*B*) Amplitudes of the three components of tail current plotted as functions of test pulse voltage. ▨, rapidly decaying component insensitive to 80 nM ω-Aga-IIIA (time constant τ = 0.47 ms); ●, rapidly decaying component blocked by 80 nM toxin (τ = 0.15 ms); ◆, slowly decaying component (τ = 3.10 ms). The parameters defining the Boltzmann distributions were: ▨, $V_{1/2}$ = −19.3 mV, k = 10.6 mV; ●, $V_{1/2}$ = 22.6 mV, k = 15.9 mV; ◆, $V_{1/2}$ = −32.7 mV, k = 5.3 mV (fit for $V_t \leq 0$ mV). Same cell as in *A*. (*C*) Current records for a holding voltage of −90 mV, a test pulse to +20 mV, and a repolarization to −50 mV: □, control (*lower trace* during the test pulse); ○, 60 nM ω-Aga-IIIA (*middle trace*); and ◇, 60 nM toxin plus 2 mM Cd (*upper trace*). Blanking interval, 150 μs; cell capacitance, 20 pF.

diastolic potentials (≈ -90 mV). When Ca currents are elicited from these more negative holding potentials, there are three distinct components of Ca channel tail current. Two of these components are rapidly decaying and represent the ionic and gating currents associated with L-type Ca channels that we have already described; the third component is slowly decaying T-type Ca channel tail current. Thus tail currents are distinctly multiexponential when they are recorded after a depolarization that opens both L- and T-type Ca channels. We like others have taken the amplitude of the slowly decaying tail current as a measure of the instantaneous

conductance of T-type Ca channels. However, a recent study of Ca channel gating currents in ventricular cells indicates that the slowly decaying component of tail current might partly represent Ca channel gating current in much the same way that the rapidly decaying component is partly due to gating current (Shirokov et al., 1992). Figs. 8 and 9 show that, in atrial myocytes, all slowly decaying tail current is due to ionic current.
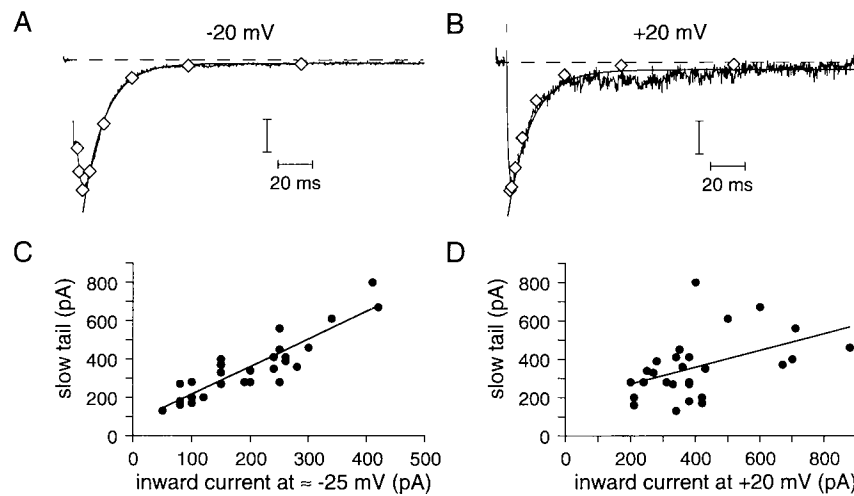

FIGURE 9. The magnitude of the slowly decaying tail current provides an accurate representation of the instantaneous conductance of T-type Ca channels. (*A* and *B*) Comparison of the slowly decaying tail current and the toxin-insensitive current during a test pulse to −20 mV (*A*) or +20 mV (*B*) from a holding voltage of −90 mV. Current traces are the current recorded during a 200-ms test pulse in the presence of 60 nM ω-Aga-IIIA (filter, 2 kHz; sampling, 4 kHz; blanking interval, 500 μs). ◇, magnitude of the slowly decaying tail current at −50 mV measured after test pulses lasting 3, 4, 6, 10, 18, 34, 66, and 130 ms (blanking interval, 250 μs, time constant, 3.0 ms). The current traces and the envelopes of tails are well fit by monoexponential decays with a time constant of (*A*) 12.5 ms and (*B*) 13.2 ms. (*Vertical calibration bar*; *A*) 173 pA for the tail currents, 91 pA for the current trace; (*B*) 370 pA for the tail currents, 25 pA for the current trace. Cell capacitance, 23 pF. (*C* and *D*) For 27 cells, the maximum magnitude of the slowly decaying tail current at −50 mV is plotted versus the amplitude of the inward Ca current at the end of a test pulse to −25 mV (*C*) or +20 mV (*D*). Test pulse, 10 ms; holding voltage, −90 mV; cell capacitances, 15–35 pF. In *C*, the data are well fit with a slope of 1.44 ($r = 0.90$, $r = 0.88$ if forced to intersect the origin). In *D*, the data are marginally fit with a slope of 0.44 ($r = 0.46$, $r < 0.20$ if forced to intersect the origin).

Fig. 8 *A* shows selective block of the rapidly decaying tail current by ω-Aga-IIIA and felodipine. As reported previously (Cohen et al., 1992*a*), ω-Aga-IIIA does not block the slowly decaying tail current due to T-type Ca channels. The toxin blocks most of the inward Ca current during the test pulse to +20 mV, leaving only the current through T-type Ca channels. The addition of 1 μM felodipine completely suppresses the remaining rapidly decaying tail current, but does not further block the current

during the test pulse to +20 mV. Although felodipine usually decreased the slowly decaying tail current in other experiments, its potency was consistently less than for block of the toxin-insensitive rapidly decaying current (Cohen et al., 1992a, b). This suggests that the two currents arise from different sources.

Fig. 8 B shows the voltage dependence of activation and the relative magnitudes of the toxin-sensitive tail current, the toxin-insensitive rapidly decaying tail current, and the slowly decaying tail current. Most of the slowly decaying tail current activates at relatively negative voltages, but activation is generally not well fit by a single two-state Boltzmann distribution; a second component activates over a voltage range similar to that for L-type Ca channel ionic current. The insensitivity of this second component to ω-Aga-IIIA and felodipine indicates that it is not due to slowly decaying L-type Ca channel ionic current ("mode 2" activity). Hence, T-type Ca channels can display complex activation kinetics similar to those found for L- and N-type Ca channels (Bean, 1989; Bean and Rios, 1989; Pietrobon and Hess, 1990).

Fig. 8 C shows superimposed current records with and without 60 nM ω-Aga-IIIA and with toxin plus 2 mM Cd. As in Fig. 8 A, ω-Aga-IIIA blocks most of the inward Ca current and part of the rapidly decaying tail current but it does not affect the slowly decaying tail. The tail current in toxin remains biexponential and Cd completely blocks the slow tail with little effect on the fast tail. Since Cd blocks ionic current through Ca channels, this result is consistent with the idea that the slowly decaying component of tail current is entirely ionic current and the rapidly decaying component is gating current.

In Fig. 9 A, the magnitudes of the slowly decaying tail currents measured after test pulses to −20 mV of various durations are compared to the amplitude of the toxin-insensitive Ca current during a single long pulse to −20 mV: they are proportional at all times. In Fig. 9 B, the same comparison is presented for test pulses to +20 mV with the same result. In Fig. 9, C and D, we have plotted the maximum magnitude of the slowly decaying tail current for 27 myocytes versus the corresponding amplitude of the Ca current at the end of a 10-ms test pulse to −25 and +20 mV, respectively. We have previously shown that current measured at −25 mV is almost entirely T-type, while current at +20 mV is almost entirely L-type (Cohen et al., 1992a). The slowly decaying tail current is proportional to the amplitude of the T-type Ca channel ionic current ($r = 0.90$), but not to the amplitude of the L-type Ca channel ionic current ($r = 0.46$). Thus, Fig. 9 shows that the amplitude of the slowly decaying component of tail current is proportional to the instantaneous conductance of T-type Ca channels. Taken in conjunction with Fig. 8 C, this result indicates that this component of tail current is entirely due to ionic current through deactivating T-type Ca channels and does not arise from intramembrane charge movement.

DISCUSSION

ω-Aga-IIIA is the only known agent that selectively blocks ionic current through L-type Ca channels in myocardial cells. We previously demonstrated that it blocks all L-type Ca channel ionic current without effect on T-type Ca channel current (Cohen et al., 1992a) and we now show that it has no effect on DHP-sensitive intramembrane charge movements. ω-Aga-IIIA is thus a valuable tool for quantifying L-type Ca

channel currents. Intramembrane charge movements constitute a significant component of total current when physiologically relevant concentrations of charge carrier are used, and thereby obscure the activation and deactivation of L-type Ca channel ionic currents (see also Hadley and Lederer, 1991). The use of ω-Aga-IIIA makes it possible to resolve the entire time course of L-type Ca channel currents in physiological concentrations of Ca.

Our studies provide a rigorous validation of tail current analysis to quantify L- and T-type Ca channel currents in myocardial cells. Unless high concentrations of charge carrier are used to augment the size of ionic currents, there are three significant components of tail current in myocardial cells: L- and T-type Ca channel ionic currents and L-type Ca channel gating current (see also Hadley and Lederer, 1991). We find that the toxin-sensitive rapidly decaying tail current accurately reflects the conductance of L-type Ca channels, while the slowly decaying tail current observed for holding potentials ≤ −50 mV is due entirely to T-type Ca channels. Thus, all of the Ca channel current can be accounted for by these two channel types.

ω-Aga-IIIA allows the isolation of DHP-sensitive intramembrane charge movements. We have obtained compelling evidence that the rapidly decaying toxin-insensitive tail current is intramembrane charge movement and not ionic current: this current is observed in the absence of ionic current during the preceding depolarization, it is insensitive to block by Cd, and the charge moved is equal and of opposite sign to charge moved during the transient outward current at the beginning of the depolarization. There are several lines of evidence indicating that these charge movements are associated with the gating of L-type Ca channels. First, Q_{on} and Q_{off} are blocked by 1 μM felodipine; DHPs are known to suppress L-type Ca channel ionic currents and this intramembrane charge movement in parallel (Field et al., 1988; Bean and Rios, 1989; Hadley and Lederer, 1991; Shirokov et al., 1992). DHPs can also be high-affinity blockers of the voltage sensor for calcium release from the sarcoplasmic reticulum in skeletal muscle (Rios and Pizarro, 1991). However, in contrast to skeletal muscle, L-type Ca channels account for nearly all myocardial DHP binding sites (Lew, Hryshko, and Bers, 1991; Rose, Balke, Wier, and Marban, 1992) and Ca release from the cardiac sarcoplasmic reticulum is Ca-induced rather than voltage-gated (Beukelmann and Wier, 1988; Niggli and Lederer, 1990; Cleemann and Morad, 1991). Thus, there is no evidence in myocardial cells for substantial DHP-sensitive charge movement associated with calcium release from the sarcoplasmic reticulum. Also, 1 μM felodipine probably does not block gating currents associated with Na channels. When Ca currents are elicited from holding potentials more negative than −50 mV, Q_{on} is of greater magnitude than Q_{off} (Fig. 8) due in part to Na channel gating current (Bean and Rios, 1989; Hanck, Sheets, and Fozzard, 1990; Josephson and Sperelakis, 1992). Felodipine has only a small effect on this larger charge movement (Fig. 8 C).

Similar DHP-sensitive charge movements are found in guinea pig tracheal myocytes, which lack Na channels but have large L-type Ca channel currents (Fig. 6). The $α_1$ subunit of the L-type Ca channel in airway smooth muscle differs from that found in cardiac myocytes in only four regions and none of these includes the presumed voltage sensor for gating or the DHP binding site (Biel, Ruth, Bosse, Hullin, Stuhmer, Flockerzi, and Hofmann, 1990; Nakayama, Taki, Striessnig, Glossmann,

Catterall, and Kanaoka, 1991). Hence, gating currents associated with L-type Ca channels in atrial and tracheal myocytes are expected to be similar. The close agreement that we found (Figs. 4 and 6) suggests that our measurements in atrial cells are minimally contaminated with charge movements associated with other voltage sensors.

Another argument in favor of identifying the asymmetric charge movement with L-type Ca channel gating current is that it has appropriate time and voltage dependences (Armstrong, 1981). Q_{on} and Q_{off} activate at more negative potentials than L-type Ca channel ionic current (Fig. 4). This is expected if a series of voltage-dependent molecular transitions precede channel opening, as suggested by the sigmoid onset of channel opening (Fig. 5) and by the first latency distribution derived from single-channel analysis (Hess, Lansman, and Tsien, 1984; Rose et al., 1992). Q_{on} is complete at the time of peak inward L-type Ca channel ionic current and $I_{g,off}$ decays more slowly than L-type Ca channel ionic tail currents (Figs. 1 and 5). If repolarization results in the reverse transition between closed states, then gating current should decay more slowly than L-type Ca channel ionic tail current (Armstrong, 1981). The decay of $I_{g,off}$ is well described by a single exponential with the same time constant following test pulses that cover a broad voltage range, suggesting that the charge movement is primarily due to one type of voltage sensor and that errors due to series resistance are small. The time course of $I_{g,on}$ suggests that activation consists of fast and slow transitions between multiple preactivated states, as found for squid axon Na channels (Vandenberg and Bezanilla, 1991). The curve fitting procedure shown in Fig. 5 is based on the assumption that one or more fast steps precede three equivalent slower steps. This model predicts that the time constant of activation of ionic current (τ_m) should be the same as the time constant of the slowly decaying component of $I_{g,on}$. We find a good correlation (Fig. 5). It is reasonable that $I_{g,on}$ has a time course similar to Na channel gating current because L-type Ca channels and Na channels have extensive structural homology (Mikami, Imoto, Tanabe, Niidome, Mori, Takeshima, Narumiya, and Numa, 1989). The multiexponential decay of $I_{g,on}$ is consistent with the finding that the four structural domains of L-type Ca channels are not equivalent in gating properties (Tanabe, Adams, Numa, and Beam, 1991). The ratio between the time constants of decay of $I_{g,off}$ and of the corresponding Ca channel ionic tail current is at least 2.2, whereas it is ≈ 1 for Na channels (Armstrong, 1981). Thus, the time course of $I_{g,off}$ is also consistent with modified Hodgkin-Huxley kinetics with three equivalent transitions necessary for channel opening; these steps are preceded by additional faster transitions.

The time course of the gating current in this study differs significantly from previous work using ventricular cells or cardiac L-type Ca channels expressed in dysgenic muscle cells. We find that $I_{g,on}$ has either no rising phase or one that is complete in 200 μs. In contrast, rising phases that last ≥ 1 ms have been reported in guinea pig and chick ventricular cells (Josephson and Sperelakis, 1991; Shirokov et al., 1992). The decay of $I_{g,on}$ is described by two exponentials in our studies but only one in previous studies; we find significantly faster rates of decay of $I_{g,off}$ and the L-type Ca channel ionic tail current than in previous studies (Hadley and Lederer, 1989; Adams, Tanabe, Mikami, Numa, and Beam, 1990; Shirokov et al., 1992). Most

of these differences could be due to a wider bandwidth of current measurements in our experiments. Mammalian ventricular cells are less suited for wide-bandwidth voltage clamp measurements with the whole-cell patch electrode technique because many of the calcium channels are in the membrane of the transverse tubules (Doyle, Kamp, Palfrey, Miller, and Page, 1986). Delays in stepping the voltage in these membranes can artificially produce a rising phase in the gating current and can slow tail currents (Simon and Beam, 1985). The differences may also occur because most previous studies used more negative holding potentials, revealing additional gating transitions. Also, in these studies, Cd or other transition metals were used to block Ca currents and these metals might alter the kinetics of charge movement when present at millimolar concentrations. We did not find evidence for very slowly decaying $I_{g,off}$ (called "charge 2"), as found with ventricular cells (Shirokov et al., 1992). This difference could be due to our use of atrial cells, which generally have a smaller Q_{max} than ventricular cells and have more T-type Ca channels. $I_{g,off}$ has a maximal amplitude of ≈ 100 pA in our studies; if it were entirely converted to charge 2 with a time constant of decay of ≈ 4 ms, then the amplitude would be ≈ 10 pA. This would be hard to detect even if almost all T-type Ca channels were inactivated (Fig. 9).

We demonstrate a much larger separation than previously reported between the Boltzmann distribution describing activation of gating charge movement and that describing activation of ionic current (Field et al., 1988; Hadley and Lederer, 1991; Josephson and Sperelakis, 1992). Part of the difference between our results and previous studies with ventricular cells may occur because we study gating and ionic currents under nearly identical ionic conditions. Also, the time constant of settling of the voltage clamp causes an error in the measurement of the steady-state activation of the toxin-sensitive tail current. Since the onset of deactivation is more delayed after stronger depolarizations, a Boltzmann fit of the true steady-state activation has a more negative midpoint and a steeper slope than shown in Fig. 4. We estimated the possible magnitude of this error by numerical simulation and found maximal changes of 5 mV for the mid-point and 1 mV for the slope factor. We also attempted to calculate the steady-state activation of the toxin-sensitive current based on the measurements of L-type Ca channel ionic current during the test depolarization. Using the Goldman-Hodgkin-Katz constant field equation (Hille, 1992), we calculated a midpoint of 16.4 mV and a slope factor of 8.5 mV for the experiment shown in Fig. 4. This midpoint is in reasonable agreement with the possible range found from the tail current measurements (18.0–23.0 mV). In contrast, the calculated slope is much smaller than the value from the tail current measurements (13.2–14.2 mV). There are at least two possible explanations of this discrepancy. First, L-type Ca channels might not obey the assumptions of the constant field equation; in particular, the condition of independence is likely to be invalid. Second, the external solution contains 0.5 mM Mg, which blocks L-type Ca channels in a voltage-dependent manner (Lansman et al., 1986); since block decreases as test pulse voltage increases, the steady-state activation calculated from current during the test depolarization would be artificially steepened.

Thus, the large voltage shift between activation of gating charge movement and ionic current is obtained either from measurements during the test depolarization or from tail currents. This shift indicates that substantial charge movement occurs prior

to channel opening. However, various isoforms of the L-type Ca channel expressed in dysgenic muscle give dramatically different separations between the activation of charge movement and activation of ionic current (Adams et al., 1990). This suggests that the penultimate step before opening is very variable in its voltage dependence.

Among different cells, Q_{max} is not proportional to the amplitude of the L-type Ca channel ionic current, in contrast to studies of Na channel gating currents (Hanck et al., 1990). This variability is not unexpected since L-type Ca channels can go through gating transitions without opening (Hadley and Lederer, 1991). We find that $Q_{max} \approx$ 4 nC/μF, consistent with studies using ventricular cells, in which Q_{max} ranges from 4 to 11 nC/μF (Field et al., 1988; Hadley and Lederer, 1989; Shirokov et al., 1992). As in these earlier studies, this amount of gating charge is surprisingly large based on early estimates of the density of calcium channels and the steepness of the voltage dependence of activation (Bean and Rios, 1989; Hadley and Lederer, 1991; Josephson and Sperelakis, 1992). However, the density of Ca channels in ventricular cells (≈ 18 channels/μm^2) is much greater than originally thought because the maximal probability of opening is much less than 1 (Lew et al., 1991). In addition, the maximal gating charge necessary to open Ca channels may be substantially greater than estimated from the slope of the activation curve, as found for structurally homologous *Shaker* potassium channels (Schoppa, McCormack, Tanyouye, and Sigworth, 1992). If we assume that the density of Ca channels in atrial cells is the same as in rabbit ventricular cells and that the maximal charge movement per channel is the same as for *Shaker* potassium channels (≈ 12 elementary charges per channel), then we expect $Q_{max} \approx 3.4$ nC/μF. Hence, our values for Q_{max} are not inconsistent with the idea that all the DHP-sensitive charge movement is due to Ca channel gating current.

ω-Aga-IIIA does not modify the DHP-sensitive gating current. Block of L-type Ca channels by toxin is not time- or voltage-dependent, suggesting that there is no interaction with channel gating (Cohen et al., 1992a). $I_{g,on}$ can be isolated without toxin at the reversal potential for ionic current or by use of Cd and this current is unaffected by ω-Aga-IIIA (see Fig. 7). Since ω-Aga-IIIA presumably has a net charge of $\approx +6$ (Venema, Swiderek, Lee, Hathaway, and Adams, 1992), the lack of effect of toxin on gating current suggests that mobile parts of the activation gate are near the cytoplasmic end of the channel and are therefore shielded from toxin. It is presently quite difficult to obtain ω-Aga-IIIA because *Agelenopsis aperta* venom is in limited supply, relatively expensive, and ω-Aga-IIIA constitutes only $\approx 1\%$ of the venom protein. We find that 100 μM Cd is a good substitute for isolating Q_{on} but not Q_{off} (Fig. 7).

In summary, there is strong evidence that in non-neuronal cells, ω-Aga-IIIA blocks all L-type Ca channel ionic current and only this current. Our results indicate that this toxin would isolate gating current associated with L-type Ca channels in a cell that expressed only this one type of voltage-gated ion channel. It is likely that we have isolated this gating current in atrial cells by using a restricted range of holding potentials, but it is not possible to exclude small contributions of intramembrane charge movement from other sources. Thus, the interaction of ω-Aga-IIIA with L-type Ca channels is similar to that of tetrodotoxin with neuronal Na channels. Both toxins block ionic current through the target channel with high affinity at all voltages,

but have little or no effect on the associated gating current. In contrast, the DHPs suppress ionic current and gating current in parallel.

Note added in proof: Neely, Wei, Olcese, Birnbaumer, and Stefani (1993) have recorded gating currents associated with α_1 and β subunits of cardiac L-type Ca channels expressed in oocytes. They report a time course for $I_{g,on}$ similar to that shown in our study.

REFERENCES

Adams, B. A., T. Tanabe, A. Mikami, S. Numa, and K. G. Beam. 1990. Intramembrane charge movement restored in dysgenic skeletal muscle by injection of dihydropyridine receptor cDNAs. *Nature.* 346:569–572.

Armstrong, C. M. 1981. Sodium channels and gating currents. *Physiological Reviews.* 61:644–683.

Armstrong, C. M., and G. Cota. 1990. Modification of sodium channel gating by lanthanum: some effects that cannot be explained by surface charge theory. *Journal of General Physiology.* 96:1129–1140.

Bean, B. P. 1989. Neurotransmitter inhibition of neuronal calcium currents by changes in channel voltage dependence. *Nature.* 340:153–156.

Bean, B. P., and E. Rios. 1989. Nonlinear charge movement in mammalian cardiac ventricular cells. *Journal of General Physiology.* 94:65–93.

Beukelmann, D. J., and W. G. Wier. 1988. Mechanism of release of calcium from sarcoplasmic reticulum of guinea-pig cardiac cells. *Journal of Physiology.* 405:233–255.

Bezanilla, F. 1985. Gating of sodium and potassium channels. *Journal of Membrane Biology.* 88:97–111.

Biel, M., P. Ruth, E. Bosse, R. Hullin, W. Stuhmer, V. Flockerzi, and F. Hofmann. 1990. Primary structure and functional expression of a high voltage activated calcium channel from rabbit lung. *FEBS Letters.* 269:409–412.

Byerly, L., P. B. Chase, and J. H. Stimers. 1984. Calcium current activation kinetics in neurones of the snail *Lymnaea stagnalis. Journal of Physiology.* 348:187–207.

Carbone, E., and H. D. Lux. 1987. Kinetics and selectivity of a low-voltage activated calcium current in chick and rat sensory neurons. *Journal of Physiology.* 386:547–570.

Chow, R. H. 1991. Cadmium block of squid calcium currents: macroscopic data and a kinetic model. *Journal of General Physiology.* 98:751–770.

Clapp, L. H., and A. M. Gurney. 1991. Outward currents in rabbit pulmonary artery cells dissociated with a new technique. *Experimental Physiology.* 76:677–693.

Cleemann, L., and M. Morad. 1991. Role of Ca^{2+} channel in cardiac excitation-contraction coupling in the rat: evidence from Ca^{2+} transients and contraction. *Journal of Physiology.* 432:283–312.

Cohen, C. J., E. A. Ertel, M. M. Smith, V. J. Venema, M. E. Adams, and M. D. Leibowitz. 1992a. High affinity block of myocardial L-type Ca channels by the spider toxin ω-Aga-IIIA: advantages over 1,4-dihydropyridines. *Molecular Pharmacology.* 42:947–951.

Cohen, C. J., R. T. McCarthy, P. Q. Barrett, and H. Rasmussen. 1988. Ca channels in adrenal glomerulosa cells: K^+ and angiotensin II increase T-type Ca channel current. *Proceedings of the National Academy of Sciences.* 85:2412–2416.

Cohen, C. J., S. Spires, and D. Van Skiver. 1992b. Block of T-type Ca channels in guinea pig atrial cells by antiarrhythmic agents and calcium channel antagonists. *Journal of General Physiology*. 100:703–728.

Cota, G. 1986. Calcium channel currents in pars intermedia cells of the rat pituitary gland: kinetic properties and washout during intracellular dialysis. *Journal of General Physiology*. 88:83–105.

Doyle, D. D., T. J. Kamp, H. C. Palfrey, R. J. Miller, and E. Page. 1986. Separation of cardiac plasmalemma into cell surface and T-tubular components: distribution of saxitoxin- and nitrendipine-binding sites. *Journal of Biological Chemistry*. 261:6556–6563.

Ertel, E. A., V. A. Warren, M. E. Adams, P. R. Griffin, C. J. Cohen and M. M. Smith. 1994. The type III ω-agatoxins: a family of probes for similar binding sites on L- and N-type calcium channels. *Biochemistry*. In press.

Field, A. C., C. Hill, and G. D. Lamb. 1988. Asymmetric charge movement and calcium currents in ventricular myocytes of neonatal rat. *Journal of Physiology*. 406:277–297.

Hadley, R. W., and W. J. Lederer. 1989. Intramembrane charge movement in guinea pig and rat ventricular myocytes. *Journal of Physiology*. 415:601–624.

Hadley, R. W., and W. J. Lederer. 1991. Properties of L-type calcium channel gating current in isolated guinea pig ventricular myocytes. *Journal of General Physiology*. 98:265–285.

Hamill, O. P., A. Marty, E. Neher, B. Sakmann, and F. J. Sigworth. 1981. Improved patch-clamp techniques for high-resolution current recording from cells and cell-free membrane patches. *Pflügers Archiv*. 391:85–100.

Hanck, D. A., M. F. Sheets, and H. A. Fozzard. 1990. Gating currents associated with Na channels in canine cardiac Purkinje cells. *Journal of General Physiology*. 95:439–457.

Hess, P., J. B. Lansman, and R. W. Tsien. 1984. Different modes of Ca channel gating behaviour favored by dihydropyridine Ca agonists and antagonists. *Nature*. 311:538–544.

Hille, B. 1992. Ionic Channels of Excitable Membranes. Sinauer Associates, Sunderland, MA.

Hiriart, M., and D. R. Matteson. 1988. Na channels and two types of Ca channels in rat pancreatic B cells identified with the reverse hemolytic plaque assay. *Journal of General Physiology*. 91:617–639.

Josephson, I. R., and N. Sperelakis. 1991. Phosphorylation shifts the time-dependence of cardiac Ca^{++} channel gating currents. *Biophysical Journal*. 60:491–497.

Josephson, I. R., and N. Sperelakis. 1992. Kinetic and steady-state properties of Na$^+$ channel and Ca^{2+} channel charge movements in ventricular myocytes of embryonic chick heart. *Journal of General Physiology*. 100:195–216.

Kostyuk, P. G., and R. E. Shirokov. 1989. Deactivation kinetics of different components of calcium inward current in the membrane of mice sensory neurones. *Journal of Physiology*. 409:343–355.

Lansman, J. B., P. Hess, and R. W. Tsien. 1986. Blockade of current through single calcium channels by Cd^{2+}, Mg^{2+}, and Ca^{2+}. Voltage and concentration dependence of calcium entry into the pore. *Journal of General Physiology*. 88:321–347.

Lew, W. Y. W., L. V. Hryshko, and D. M. Bers. 1991. Dihydropyridine receptors are primarily functional L-type Ca channels in rabbit ventricular myocytes. *Circulation Research*. 69:1139–1145.

Matteson, D. R., and C. M. Armstrong. 1986. Properties of two types of calcium channels in clonal pituitary cells. *Journal of General Physiology*. 87:161–182.

McCarthy, R. T., and C. J. Cohen. 1989. Nimodipine block of calcium channels in rat vascular smooth muscle cell lines: exceptionally high affinity binding in A7r5 and A10 cells. *Journal of General Physiology*. 94:669–692.

Mikami, A., K. Imoto, T. Tanabe, T. Niidome, Y. Mori, H. Takeshima, S. Narumiya, and S. Numa. 1989. Primary structure and functional expression of the cardiac dihydropyridine-sensitive calcium channel. *Nature*. 340:230–233.

Mintz, I. M., V. J. Venema, M. E. Adams, and B. P. Bean. 1991. Inhibition of N- and L-type Ca^{2+} channels by the spider venom toxin ω-Aga-IIIA. *Proceedings of the National Academy of Sciences.* 88:6628–6631.

Mitra, R., and M. Morad. 1985. A uniform enzymatic method for dissociation of myocytes from hearts and stomachs of vertebrates. *American Journal of Physiology.* 249:H1056–H1060.

Nakayama, H., M. Taki, J. Striessnig, H. Glossmann, W. A. Catterall, and Y. Kanaoka. 1991. Identification of 1,4-dihydropyridine binding regions within the α1 subunit of skeletal muscle Ca^{2+} channels by photoaffinity labeling with diazipine. *Proceedings of the National Academy of Sciences.* 88:9203–9207.

Neely, A., X. Wei, R. Olcese, L. Birnbaumer, and E. Stefani. 1993. Potentiation by the β subunit of the ratio of the ionic current to the charge movement in the cardiac calcium channel. *Science.* 262:575–578.

Niggli, E., and W. J. Lederer. 1990. Voltage-independent calcium release in heart muscle. *Science.* 250:565–568.

Nyborg, N. C. B. and M. J. Mulvany. 1984. Effect of felodipine, a new dihydropyridine vasodilator, on contractile responses to potassium, noradrenaline, and calcium in mesenteric resistance vessels of the rat. *Journal of Cardiovascular Pharmacology.* 6:499–505.

Pietrobon, D., and P. Hess. 1990. Novel mechanism of voltage dependent gating in L-type calcium channels. *Nature.* 346:651–655.

Press, W. H., B. P. Flannery, S. A. Teukolsky, and W. T. Vetterling. 1986. Numerical Recipes. Cambridge University Press, Cambridge, UK.

Rios, E., and G. Pizarro. 1991. Voltage sensor of excitation-contraction coupling in skeletal muscle. *Physiological Reviews.* 71:849–908.

Rose, W. C., C. W. Balke, W. G. Wier, and E. Marban. 1992. Macroscopic and unitary properties of physiological ion flux through L-type Ca^{2+} channels in guinea pig heart cells. *Journal of Physiology.* 456:267–284.

Schoppa, N. E., K. McCormack, M. A. Tanyouye, and F. J. Sigworth. 1992. The size of gating charge in wild-type and mutant *Shaker* potassium channels. *Science.* 255:1712–1715.

Sheets, M. F., and D. A. Hanck. 1992. Mechanisms of extracellular divalent and trivalent cation block of the sodium current in canine cardiac Purkinje cells. *Journal of Physiology.* 454:299–320.

Shirokov, R., R. Levis, N. Shirokova, and E. Rios. 1992. Two classes of gating current from L-type Ca channels in guinea pig ventricular myocytes. *Journal of General Physiology.* 99:863–895.

Simon, B. J., and K. G. Beam. 1985. The influence of transverse tubular delays on the kinetics of charge movement in mammalian skeletal muscle. *Journal of General Physiology.* 85:21–42.

Tanabe, T., B. A. Adams, S. Numa, and K. G. Beam. 1991. Repeat I of the dihydropyridine receptor is critical in determining calcium channel activation kinetics. *Nature.* 352:800–803.

Vandenberg, C. A., and F. Bezanilla. 1991. A sodium channel gating model based on single channel, macroscopic ionic, and gating currents in the squid giant axon. *Biophysical Journal.* 60:1511–1533.

Venema, V. J., K. M. Swiderek, T. D. Lee, G. M. Hathaway, and M. E. Adams. 1992. Antagonism of synaptosomal calcium channels by subtypes of ω-agatoxins. *Journal of Biological Chemistry.* 267:2610–2615.

Warshaw, D. M., J. L. Szarek, M. S. Hubbard, and J. N. Evans. 1986. Pharmacology and force development of single freshly isolated bovine carotid artery smooth muscle cells. *Circulation Research.* 58:399–406.

Yue, D. T., and E. Marban. 1990. Permeation in the dihydropyridine-sensitive calcium channel. Multi-ion occupancy but no anomalous mole-fraction effect between Ba^{2+} and Ca^{2+}. *Journal of General Physiology.* 95:911–939.